International Journal of Modern Physics B
Vol. 29, No. 1 (2015) 1530001 (22 pages)

DOI: 10.1142/S0217979215300017

World Scientific
www.worldscientific.com

Topological Fulde–Ferrell superfluids of a spin–orbit coupled Fermi gas

Yong Xu* and Chuanwei Zhang†

Department of Physics, The University of Texas at Dallas, Richardson, Texas 75080, USA
**yongxuphy@gmail.com*
†chuanwei.zhang@utdallas.edu

Received 19 October 2014
Accepted 24 November 2014
Published 12 December 2014

Topological Fermi superfluids have played the central role in various fields of physics. However, all previous studies focus on the cases where Cooper pairs have zero center-of-mass momenta (i.e., normal superfluids). The topology of Fulde–Ferrell (FF) superfluids with nonzero momentum pairings have never been explored until recent findings that FF superfluids in a spin–orbit (SO) coupled Fermi gas can accommodate Majorana fermions in real space in low dimensions and Weyl fermions in momentum space in three dimension. In this review, we first discuss the mechanism of pairings in SO coupled Fermi gases in optical lattices subject to Zeeman fields, showing that SO coupling as well as Zeeman fields enhance FF states while suppress Larkin–Ovchinnikov states. We then present the low temperature phase diagram including both FF superfluids and topological FF superfluids phases in both two dimension and three dimension. In one dimension, Majorana fermions as well as phase dependent order parameter are visualized. In three dimension, we show the properties of Weyl fermions in momentum space such as anisotropic linear dispersion, Fermi arch, and gaplessness away from $k_\perp = 0$. Finally, we discuss some possible methods to probe FF superfluids and topological FF superfluids in cold atom systems.

Keywords: Fulde–Ferrell superfluids; Majorana fermions; Weyl fermions; spin–orbit coupling.

PACS numbers: 03.75.Ss, 03.75.Lm, 05.30.Fk

1. Introduction

The exotic Fulde–Ferrell–Larkin–Ovchinnikov (FFLO) state was proposed as the ground state for a superconductor with strong Zeeman splitting about half a century ago.[1,2] The Cooper pairs of such states have finite center-of-mass momenta with the spatially dependent order parameter, instead of zero momenta with the spatially uniform order parameter in normal superconductors. To date, intense search has

been undertaken in solid materials such as heavy-fermion superconductors,[3–7] organic superconductors,[8–11] iron pnictide superconductors[12,13] and two-dimensional (2D) electron gases.[14] Despite some remarkable findings, conclusive evidence has not been observed. The realization of ultralcold atom systems provides a disorder-free and highly controllable platform to simulate quantum phenomena. In this system, FFLO states have been predicted to exist in a polarized Fermi gas[15–17] as well as a polarized fermionic optical lattice,[18–24] where the polarization can be readily tuned by the particle number difference of two component fermions. The phase diagram where the FFLO states occupy is much larger in 1D or quasi-1D[25–35] than that in 3D due to a nesting effect.[36] In experiments, the Hulet group[37] has measured the density profiles of an imbalanced two component mixture of ultralcold ^{6}Li atoms in a quasi-1D geometry, showing a partially polarized core surrounded by paired or fully polarized shells, in good agreement with theoretical calculations.[25,26] However, the superfluidity of the polarized core has not been detected, leaving the FFLO superfluids still ambiguous.

Majorana fermions, quantum particles which are their own anti-particles, have been the focus of many theorists and experimentalists in superconductivity/superfluidity because of their tantalizing properties[38–51] and potential applications in fault-tolerant quantum computation.[52] Majorana fermions generally locate at the defects such as vortices, edges and domain walls in real space in low-dimensions as zero energy quasiparticle excitations. Interestingly, another type of topological fermions, Weyl fermions,[53] can also exist as quasiparticle excitations in superfluids, not in real space of low-dimensional systems but in momentum space of three-dimensional (3D) ones. Such superfluids include ^{3}He A phase,[54] spin–orbit (SO) coupled Fermi gases,[55,56] SO coupled Fulde–Ferrell (FF) superfluids[57,58] and dipolar Fermi gases.[59] Weyl fermions are massless chiral Dirac fermions in 3D momentum space with linear energy dispersion. Such fermions are robust and can only be destroyed by merging two Weyl fermions with opposite charges, in sharp contrast to its analog in 2D, Dirac fermions (e.g., graphene) whose gap can be opened by the perturbation breaking time-reversal symmetry or space inversion symmetry.

The realization of SO coupling in cold atom systems[60–66] has provided neutral atoms an opportunity to exhibit intriguing ground states both in Boson and Fermi gases,[67–70] which are remarkably different from those without the SO coupling. In Boson gases, the ground state can be stripe or plane wave[71–76] for repulsive interactions and can be bright solitons with spin parity symmetry for attractive interactions.[77,78] The shape of such bright solitons depends on their velocity because of the breaking of Galilean invariance.[77,79] These intriguing ground states are mainly due to the appearance of a double well structure of the underlying single particle spectrum. In Fermi gases, the ground state of superfluids with SO coupling can become topological in the presence of out-of-plane Zeeman fields and such topological superfluids accommodate Majorana fermions in low dimensions[80–88] or Weyl fermions in 3D.[55,56] Recently, such SO coupled superfluids with in-plane Zeeman

splitting have been found to support FF states, which are dominant in the low temperature phase diagram.[89–97] The competition between Larkin–Ovchinnikov (LO) and FF states was examined and the pairing mechanism was discussed in optical lattices.[98] Later, it was found that in the presence of both in-plane and out-of-plane Zeeman fields the FF superfluids can become topological in low dimensions as well as 3D and support Majorana fermions[99–102] and anisotropic Weyl fermion excitations,[57,58] respectively.

In this review, we will present some essential aspects of topological FF superfluids. In Sec. 2, we discuss the effects of Zeeman fields on the single particle spectrum of SO coupled Fermi gases and the mechanism of FF Cooper pairings. In Sec. 3, we describe the topological properties of FF superfluids in 1D, 2D and 3D. We also discuss the feasibility to observe the topological FF superfluids by speeds of sound.

2. Single Particle Picture and Pairing Mechanism

We first consider the effects of SO coupling and Zeeman fields on the single particle spectrum. The single particle Hamiltonian can be written as

$$H_s(\hat{\mathbf{p}}) = \frac{\hat{\mathbf{p}}^2}{2m} - \mu + H_{\rm SOC}(\hat{\mathbf{p}}) + H_z \tag{1}$$

with momentum operator $\hat{\mathbf{p}} = -i\hbar(\partial_x \mathbf{e}_x + \partial_y \mathbf{e}_y)$, chemical potential μ and the atom mass m. The Rashba SO coupling $H_{\rm SOC}(\hat{\mathbf{p}}) = \alpha(\hat{\mathbf{p}} \times \boldsymbol{\sigma}) \cdot \mathbf{e}_z$ with Pauli matrix $\boldsymbol{\sigma}$; the Zeeman field $H_z = h_x\sigma_x + h_z\sigma_z$ along the x (in-plane) and z (out-of-plane) directions. In the presence of SO coupling, spin is no longer a good quantum number, but replaced by the helical index (eigenvalue of $((\hat{\mathbf{p}} \times \boldsymbol{\sigma}) \cdot \mathbf{e}_z)/|p|$). Here we consider Rashba SO coupling, so that the kinetic energy term along the z-direction can be incorporated into the chemical potential and this does not change the single particle physics and relevant pairing mechanism. Thus here we focus on 2D. This Hamiltonian is readily diagonalized in momentum space. It is evident that the energy spectrum has the rotational symmetry, which cannot be broken by out-of-plane Zeeman fields. However, in-plane Zeeman fields are capable of breaking this symmetry. We define two operators $U_x = \sigma_y\mathcal{T}$ and $U_y = \sigma_x\mathcal{T}$ where $\mathcal{T}$ is the time reversal operator. It can be easily seen that with an in-plane Zeeman field (h_x) along the x-direction, the symmetry defined by U_x is satisfied that $U_x H_s(\hat{\mathbf{p}})U_x^{-1} = H_s(\hat{p}_x, -\hat{p}_y)$ leading to $E(-k_x, k_y) = E(k_x, k_y)$. However, the symmetry defined by U_y is broken, generally leading to $E(k_x, -k_y) \neq E(k_x, k_y)$. When the in-plane Zeeman field is along the y-direction, the opposite is true.

To be specific, the energy spectrum reads

$$E(\mathbf{k}) = \frac{\hbar^2\mathbf{k}^2}{2m} \pm \sqrt{\alpha^2 k_x^2 + (h_x - \alpha k_y)^2 + h_z^2}\,, \tag{2}$$

which clearly exhibits the symmetry breaking in the presence of h_x. The effect of h_z is to open a gap between two helical branches whereas h_x cannot as shown in Fig. 1(a) and 1(b).

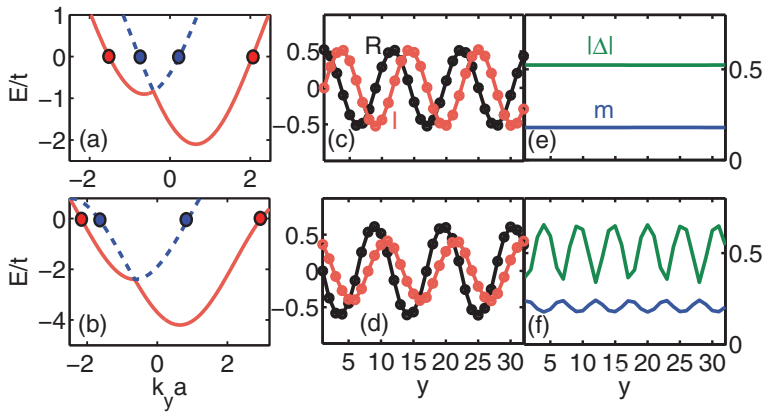

Fig. 1. (Color online) The single particle spectrum along k_y with $k_x = 0$ in (a) and (b), where the solid red and dashed blue lines represent the helicity $-$ and helicity $+$ branches respectively. The real and imaginary parts of the order parameter in (c) and (d). The absolute value of the order parameter and the magnetism in (e) and (f). The first row corresponds to a FF state, while the second a LO state.

In the following, we discuss the pairing issue in the presence of attractive interactions. One question is whether the pairing mainly occurs around the Fermi surface in the BCS regime, leading to finite center-of-mass momentum Cooper pairings (i.e., FF superfluids) because of the distortion of the single particle spectrum. Another question is whether FF superfluids are really the ground states instead of LO superfluids. FF and LO states are two types of FFLO states associated with phase dependent order parameter $\Delta(\mathbf{r}) \propto e^{i\mathbf{Q}\cdot\mathbf{r}}$ and with amplitude oscillating order parameter $\Delta(\mathbf{r}) \propto \cos(\mathbf{Q}\cdot\mathbf{r})$, respectively. LO states can be regarded as the interference states of two Cooper pairs (two FF states) with opposite center-of-mass momenta. In a system with the inversion symmetric Fermi surface, LO states are generally energetically favorable than FF states because if there are Cooper pairs with momenta $\mathbf{Q}$, the existence of Cooper pairs with momenta $-\mathbf{Q}$ can decrease the energy.[22]

To address these crucial questions, we perform the calculation of Bogoliubov-de Gennes (BdG) equations self-consistently in the optical lattice model to gain the order parameter and the pairing density in the helical representation, since in the real space model it is not necessary to postulate the form of Cooper pairs. In optical lattices, based on tight-binding model, the Hamiltonian in momentum space can be obtained by replacing the kinetic energy and H_{SOC} with $-2t(\cos(k_x a) + \cos(k_y a))$, $\alpha(\sin(k_x a)\sigma_y - \sin(k_y a)\sigma_x)$, respectively. Here t and a are the hopping parameter and lattice constant, depending on the strength and wavelength of laser beams respectively.

To examine whether fermionic atoms form Cooper pairs around the Fermi surface in the same helical branch, Figs. 2(b) and 2(c) plot the pairing density $|\langle \hat{c}_{\mathbf{k}}, -\hat{c}_{-\mathbf{k}+Q_y,-}\rangle|^2$ and $|\langle \hat{c}_{\mathbf{k}}, +\hat{c}_{-\mathbf{k}-Q_y,+}\rangle|^2$, where $\hat{c}_{\mathbf{k},\lambda}$ annihilates an atom with

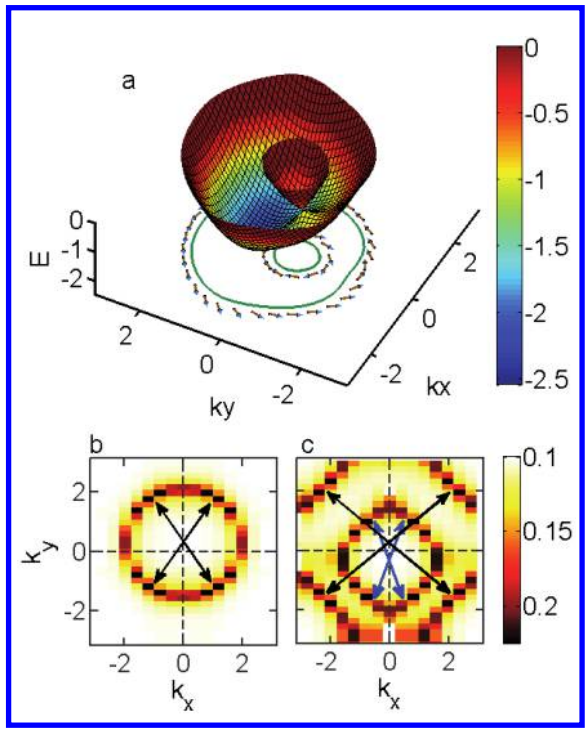

Fig. 2. (Color online) (a) Single particle band structure in momentum space for a specific FF state. The Fermi surface is plotted on the bottom layer with green line. The small arrows around the Fermi surface are the spin orientations. (b) Shows the pairing density $|\langle \hat{c}_{\mathbf{k}}, -\hat{c}_{-\mathbf{k}+Q_y,-}\rangle|^2$ for a FF state, whose single particle spectrum is plotted in (a); here $-$ indicates the lower branch. The black double arrows show the pairing. (c) presents the pairing density $|\langle \hat{c}_{\mathbf{k}}, -\hat{c}_{-\mathbf{k}+Q_y,-}\rangle|^2$, and $|\langle \hat{c}_{\mathbf{k}}, +\hat{c}_{-\mathbf{k}-Q_y,+}\rangle|^2$ for the LO phase. Here $+$ indicates the higher branch. The black and blue double arrows illustrate the Cooper pairings with Q_y and $-Q_y$, respectively. Q_y depends on the deformation of the Fermi surface by the SO coupling and the Zeeman field. The units of E, and k_x, k_y are t and $1/a$ respectively. From Ref. 98.

momentum $\mathbf{k}$ in the helical λ branch. It shows that Cooper pairs are mainly formed by the atoms around the Fermi surface in the same helical branch. The pairs possess finite momenta (thus FFLO superfluids) due to the distortion of band structure along the y-direction as shown in Fig. 2(a). In FF states, only the helical $-$ branch takes part in the pairing while the contribution of the helical $+$ branch is extremely small because of much smaller density of states. In contrast, atoms in both branches participate in the pairing for LO states.

Based on the above results, FF states are not always the ground state and LO states still have the chance to be. It mainly depends on the single particle structure and the chemical potential (see phase diagram in Ref. 98). In Fig. 1, we take two examples associated with FF and LO states, respectively to illustrate these effects. Figures 1(a) and 1(b) presents the single particle energy with respect to k_y for fixed $k_x = 0$. In the right panel, the superfluids order parameter $\Delta(i)$ calculated self-consistently in Ref. 98 is plotted. Here $\Delta(i) = U\langle \hat{c}_{i\downarrow}\hat{c}_{i\uparrow}\rangle$ with interaction

strength U, annihilation operator $\hat{c}_{i\sigma}$ at i site with spin σ. (c) and (e) have FF type pairing with space dependent phase order parameter while (d) and (f) LO type with space oscillating amplitude order parameter. Since the pairing happens in the same helical branch as red and blue points in Fig. 1(a) and 1(b), a local superfluid order parameter can be written as $\Delta_i = \Delta_- \exp(iyQ_{y-}) + \Delta_+ \exp(iyQ_{y+})$ with the former part contributed by the pairing in the helical $-$ branch and the latter one in the helical $+$ branch. When the chemical potential is placed where the density of states in the helical $+$ branch is small, $\Delta_+ \approx 0$ and $\Delta_i = \Delta_- \exp(iyQ_{y-})$, the FF pairing, as shown in the first row of Fig. 1; however, when the opposite is true as shown in the second row of Fig. 1, $\Delta_+ \neq 0$ and $Q_{y-} \approx -Q_{y+}$, leading to a LO superfluid. It is important to note that such LO states are different from the traditional LO states where the order parameter is real and has nodes. Because $|\Delta_-| > |\Delta_+|$ due to higher density of states in the helical $-$ branch, such generalized LO states are complex and have the nonzero order parameter domain walls. In general, the SO coupling and in-plane Zeeman fields enhance the FF superfluids and suppress the LO superfluids.

3. Topological FF Superfluids in SO Coupled Fermi Gases

3.1. *Model and effective Hamiltonian*

We consider a SO coupled Fermi gas subject to both in-plane and out-of-plane Zeeman fields and s-wave contact interactions. The many-body Hamiltonian can be written as

$$H = \int d\mathbf{r}\hat{\Psi}^\dagger(\mathbf{r})H_s(\hat{\mathbf{p}})\hat{\Psi}(\mathbf{r}) - U\int d\mathbf{r}\hat{\Psi}^\dagger_\uparrow(\mathbf{r})\hat{\Psi}^\dagger_\downarrow(\mathbf{r})\hat{\Psi}_\downarrow(\mathbf{r})\hat{\Psi}_\uparrow(\mathbf{r})\,, \tag{3}$$

where U characterizes the strength of attractive interactions; $\hat{\Psi}(\mathbf{r}) = [\hat{\Psi}_\uparrow(\mathbf{r}), \hat{\Psi}_\downarrow(\mathbf{r})]^T$ and $\hat{\Psi}^\dagger_\nu(\mathbf{r})$ ($\hat{\Psi}_\nu(\mathbf{r})$) is fermionic atom creation (annihilation) operator.

In quantum field theory, the partition function can be written as $Z = \mathrm{Tr}(e^{-\beta H}) = \int D(\bar{\psi},\psi)e^{-S_{\mathrm{eff}}[\bar{\psi},\psi]}$ with $\beta = 1/k_BT$. The effective action is

$$S_{\mathrm{eff}}[\bar{\psi},\psi] = \int_0^\beta d\tau\left(\int d\mathbf{r}\sum_\sigma \bar{\psi}_\sigma(\mathbf{r},\tau)\partial_\tau\psi_\sigma(\mathbf{r},\tau) + H(\bar{\psi},\psi)\right), \tag{4}$$

where $\int d\tau$ is an integral over the imaginary time τ and $H(\bar{\psi},\psi)$ is obtained by replacing $\hat{\Psi}^\dagger_\sigma$ and $\hat{\Psi}_\sigma$ with Grassman field number $\bar{\psi}_\sigma$ and ψ_σ. The quartic interaction term is transformed to quadratic one by Hubbard–Stratonovich transformation, where the order parameter $\Delta(\mathbf{r},\tau)$ is defined. By integrating out fermion fields, the partition function reads $Z = \int D(\bar{\Delta},\Delta)e^{-S_{\mathrm{eff}}[\bar{\Delta},\Delta]}$, where the effective action can be written as

$$S_{\mathrm{eff}}[\bar{\Delta},\Delta] = \int_0^\beta d\tau\int d\mathbf{r}\left(\frac{|\Delta|^2}{U}\right) - \frac{1}{2}\ln\det G^{-1}\,. \tag{5}$$

Here the inverse single particle Green function $G^{-1} = -\partial_\tau - H_B(\hat{\mathbf{p}})$ in the Nambu–Gor'kov representation with 4×4 Bogoliubov–de Gennes (BdG) Hamiltonian

$$H_B(\hat{\mathbf{p}}) = \begin{pmatrix} H_s(\hat{\mathbf{p}}) & \Delta(\mathbf{r},\tau) \\ \Delta(\mathbf{r},\tau) & -\sigma_y H_s(\hat{\mathbf{p}})^* \sigma_y \end{pmatrix}. \tag{6}$$

Based on the conclusion in the previous section that SO coupling and in-plane Zeeman fields enhance the FF states, we assume the FF form order parameter of Fermi gases, $\Delta(\mathbf{r},\tau)_0 = e^{iQ_y y}\Delta_0$ with the space independent Δ_0. By Fourier transformation and summing the Matsubara frequency, this form of $\Delta(\mathbf{r},\tau)$ yields the thermodynamical potential

$$\Omega = |\Delta|^2/U + \sum_{\mathbf{k}} (\hbar^2(-\mathbf{k}+\mathbf{Q}/2)^2/2m - \mu) - \sum_{\mathbf{k},\sigma} \frac{1}{2\beta} \ln(1 + e^{-\beta E_{\mathbf{k}\sigma}}). \tag{7}$$

Here $E_{\mathbf{k}\sigma}$ is the eigenvalue of 4×4 BdG Hamiltonian

$$H_B = \begin{pmatrix} H_s(\mathbf{k}+\mathbf{Q}/2) & \Delta_0 \\ \Delta_0 & -\sigma_y H_s(-\mathbf{k}+\mathbf{Q}/2)^* \sigma_y \end{pmatrix}, \tag{8}$$

$\mathbf{Q} = Q_y \mathbf{e}_y$ is the total momentum of the Cooper pair. The mean-field solutions of Δ_0, Q_y and μ satisfy the saddle point equations $\partial\Omega/\partial\Delta_0 = 0$, $\partial\Omega/\partial Q_y = 0$ and the atom number equation $\partial\Omega/\partial\mu = -n$ with a fixed total atom density n. To regularize the ultra-violet divergence at large $\mathbf{k}$, we follow the standard procedure[103]: in 3D $1/U = m/(4\pi\hbar^2 a_s) - \int (d\mathbf{k}/(2\pi)^3)(m/\hbar^2 k^2)$ with the s-wave scattering length a_s and in 2D $1/U = \sum_{\mathbf{k}} 1/(\hbar^2 k^2/m + E_b)$ with the binding energy E_b. The self-consistent solution is obtained through the minimization of the free energy $F = \Omega + \mu n$. The energy unit is chosen as the Fermi energy $E_F = \hbar^2 \mathbf{K}_F^2/2m$ of noninteracting Fermi gases without SO coupling and Zeeman fields with Fermi vector $K_F = (3\pi^2 n)^{1/3}$ in 3D and $K_F = (2\pi n)^{1/2}$ in 2D.

Such BdG Hamiltonian possesses the particle-hole symmetry $\Xi = \Lambda\mathcal{K}$ with $\Lambda = i\sigma_y\tau_y$, and the complex conjugate operator $\mathcal{K}$. Here $\Xi^2 = 1$. This leads to $E_{-\mathbf{k}\sigma} = -E_{\mathbf{k}\bar{\sigma}}$, where $\bar{\sigma} = 5 - \sigma$ if we label the eigenvalues from 1 to 4.

3.2. *FF superfluids*

The mean-field ground state of a SO coupled Fermi gas subject to pure in-plane Zeeman fields was first calculated in 3D in Ref. 89 and then in 2D in Ref. 90. It was found that Q_y is nonzero with nonzero Zeeman fields, implying the existence of FF parings. Q_y is also a monotonously increasing function of Zeeman fields. The phase diagram where FF states exist becomes dominant as shown in Fig. 3, in sharp contrast to traditional FFLO superfluids which can only exist in a tiny fraction of the phase diagram. The free energy difference between FF states and excited BCS states can be as large as $0.04E_F$.[89] The gapless FF superfluids with

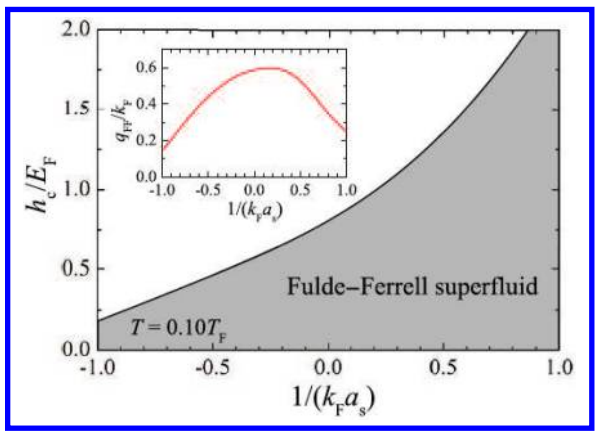

Fig. 3. Phase diagram with respect to in-plane Zeeman fields h_c across BCS–BEC crossover at low temperature $T = 0.1T_F$ (from Ref. 95).

gapless quasiparticle excitations, originating from the strong distortion of the energy excitations, have also been found.[90,94] The finite temperature mean-field phase diagram is obtained in Refs. 94 and 95, showing that FF states also dominate at finite temperature.

3.3. *Topological FF superfluids in* 1*D and* 2*D*

In the presence of out-of-plane Zeeman fields (h_z), the gap between two helical branches is opened and superfluids can become topological, which host Majorana fermions in 1D and 2D. In the following, we first briefly introduce the current progress of Majorana fermions and then discuss them in FF superfluids.

3.3.1. *Majorana fermions*

Majorana fermions, quantum particles which are their own anti-particles, have attracted tremendous interests since the Kitaev's seminal paper[104] suggested their potential applications in fault-tolerant quantum computation in 1D spinless p-wave superconductors. To date, there are lots of proposals to create Majorana fermions including 2D p_x+ip_y superconductors,[38,39] the surface of 3D topological insulators in conjunction with the proximity effect of superconductors,[40] 1D nanowire with SO coupling[42–44] and time-reversal invariant d-wave superconductors.[105–109]

In ultralcold atom systems, there are also many proposals to generate Majorana fermions ranging from 1D SO coupled Fermi gases where Majorana fermions can exit at different phase boundary[84] or inside a soliton[88] to SO coupled, staggered, and shaken optical lattices.[110–112] Here the superfluidity is generated by the intrinsic attractive interactions, not by the proximity effects. Recent experiments have shown the existence of zero energy peaks (i.e., Majorana fermions),[47–50] however, whether the zero energy excitation is caused by Majorana fermions or disorder[113] is still

under debate. In this aspect, cold atom systems are an ideal platform because of their disorder-free properties.

All the superconductors/superfluids belong to BCS pairing with zero center-of-mass momentum Cooper pairings. Refs. 99–102 suggest that FF superfluids can also become topological, supporting Majorana fermion excitations in 1D and 2D.

3.3.2. *Signature of Majorana fermions in momentum space in 2D*

We first consider a 2D Rashba SO coupled Fermi gas subject to a pure out-of-plane Zeeman field. By diagonalizing the BdG Hamiltonian in momentum space, the quasiparticle excitations can be written as

$$E_{\pm}^{\lambda}(\mathbf{k}) = \lambda\sqrt{\xi_{\mathbf{k}}^2 + \alpha^2 k^2 + h_z^2 + |\Delta_0|^2 \pm 2\sqrt{h_z^2(\xi_{\mathbf{k}}^2 + |\Delta_0|^2) + \alpha^2 k^2 \xi_{\mathbf{k}}^2}}\,, \tag{9}$$

where $\lambda = \pm$ indicating the particle and hole branches, $\xi_{\mathbf{k}} = \hbar^2\mathbf{k}^2/2m - \mu$ and $k = \sqrt{k_x^2 + k_y^2}$. Without SO coupling and Zeeman fields ($\alpha = h_z = 0$), it becomes the typical BCS superfluids excitations $E_{\mathbf{k},\pm}^{\lambda} = \lambda\sqrt{\xi_{\mathbf{k}}^2 + |\Delta_0|^2}$ with the gap $|\Delta_0|$. To obtain the gap close point in the presence of SO coupling and Zeeman fields, which generally indicates a topological phase transition, we write the multiplication of two particle branches of the quasiparticle excitations:

$$E_{+}^{+}(\mathbf{k})E_{-}^{+}(\mathbf{k}) = (h_z^2 + \alpha^2 k^2 - \xi_{\mathbf{k}}^2 - |\Delta_0|^2)^2 + 4\alpha^2 k^2 |\Delta_0|^2\,. \tag{10}$$

Clearly, the gap can only close at $k = 0$ and $h_z = \sqrt{\mu^2 + |\Delta_0|^2}$. Although the gap closing is not a sufficient condition for the topological transition, here it really indicates the transition with a sharp change of Chern number. This point also corresponds to a sharp change of the topological index $\mathcal{M} = \mathrm{sign}(\mathrm{Pf}(\Gamma))$,[114] where Pf is the Pfaffian of the skew matrix $\Gamma = H_B(0)\Lambda$ with $\Lambda = i\sigma_y\tau_y$. The appearance of the topology in a s-wave interacted Fermi gas can be understood from the analogy to a spinless p-wave Hamiltonian. In the helical representation, the effective Hamiltonian reads

$$H_{\mathrm{BdG}} = \sum_{\mathbf{k}} E_{-}(\mathbf{k})\hat{c}_{\mathbf{k}-}^{\dagger}\hat{c}_{\mathbf{k}-} + (\Delta(\mathbf{k})\hat{c}_{-\mathbf{k}-}\hat{c}_{\mathbf{k}-} + \mathrm{h.c.})\,, \tag{11}$$

where $\Delta(\mathbf{k}) = \alpha\Delta_0^* k e^{i\theta_{\mathbf{k}}}/(2\sqrt{h_z^2 + \alpha^2 k^2})$ with the angle $\theta_{\mathbf{k}}$ between $\mathbf{k}$ and k_y. This Hamiltonian is formally equivalent to a spinless $p_x + ip_y$ superconductor.[38,39]

With in-plane Zeeman fields, Refs. 99–101 found that topological FF superfluids can exist when

$$h_z{}^2 + \bar{h}_x^2 > \bar{\mu}^2 + \Delta_0^2\,, \quad \alpha h_z \Delta_0 \neq 0\,, \quad E_g > 0\,, \tag{12}$$

where $\bar{h}_x = h_x + \alpha Q_y/2$, $\bar{\mu} = \mu - Q_y^2/8m$ and E_g is the gap of the particle branches of the quasiparticle excitations. We note that this condition was generalized to the case with $E_g < 0$[115,116] after the gapless FF topological superfluids were found in 3D.[57] The nonzero value of Q_y indicates the superfluids are FF type. When $h_x = 0$ thus

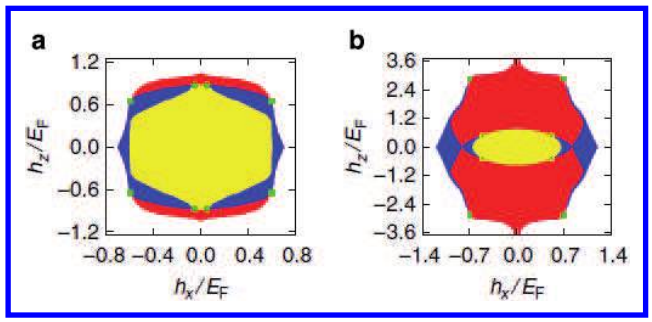

Fig. 4. (Color online) Phase diagram of FF superfluids. Red, yellow, blue and white regions correspond to topological gapped FF superfluids, nontopological gapped FF superfluids, gapless FF superfluids and normal gases, respectively. In (a), $E_b = 0.4E_F$, $\alpha K_F = 0.5E_F$; in (b), $E_b = 0.4E_F$, $\alpha K_F = 1.0E_F$. From Ref. 99.

$Q_y = 0$, this condition reduces to $h_z > \sqrt{\mu^2 + \Delta_0^2}$, the forementioned requirement for the topological phase transition. With increasing h_x, the critical h_z decreases. However, this decreasing cannot help enhance their Berezinskii–Kosterlitz–Thouless (BKT) temperatures.[117] The phase diagram in Fig. 4 presents the topological FF superfluids region (red area) in the (h_x, h_z) plane, which increases dramatically as SO coupling is enlarged.

3.3.3. *Realspace visualization of Majorana fermions in 1D*

Generally, Majorana fermions locate at the defects, such as vortices, edges, and domain walls.[38,39,83,84,88] To visualize the existence of zero Majorana fermion excitations, Refs. 99 and 102 performed the self-consistent calculation of 1D optical lattice BdG equations with the open boundary condition. Figure 5 demonstrates

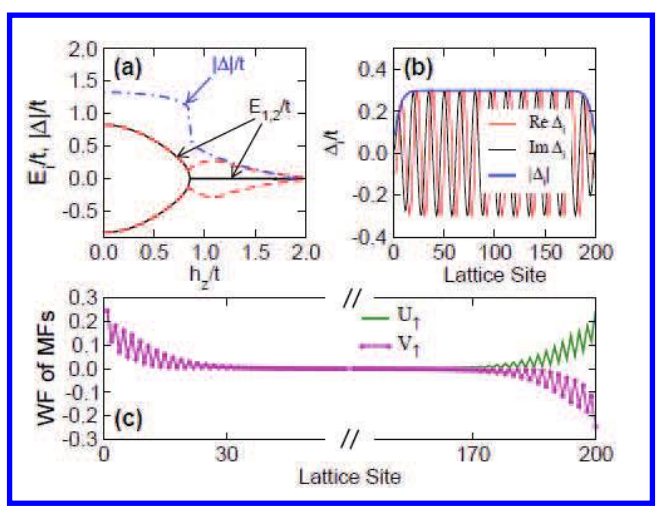

Fig. 5. (Color online) (a) Plot of the quasiparticle excitation energies and the order parameter. (b) The spatial profile of the FF type order parameter. (c) The wavefunction of the Majorana zero modes. From Ref. 99.

that zero Majorana fermion excitations, which are protected by a large gap, appear at a sufficiently large Zeeman field and the order parameter has FF type. The wavefunctions of Majorana fermions are local edge states, satisfying the self-Hermite condition.

Compared with the engineering of Majorana fermions in solid materials where the superconductivity is generally generated through proximity effects, the superfluid order parameter is created by intrinsic attractive interactions. The problem is that such low-dimensional systems cannot undergo conventional phase transition to a state with long-range order, raising the concerns whether Majorana fermions can exist in 1D and 2D Fermi gases. In 1D, Refs. 118 and 119 examined this problem and found that Majorana fermions can also exist in a 1D system with algebraically decaying superconducting fluctuations. Fluctuations may also be suppressed in a quasi-1D system, where the long range order can be restored by the existence of other dimensions albeit small.[27]

In 2D, the relevant physics is the BKT transition[120–122] to a state with quasi-long-range order (i.e., vortex-antivortex (V-AV) pairs),[86,123–125] with the critical temperature determined by the superfluid density tensor. Reference 86 suggested that Majorana fermions can only be observed at finite temperature in the sense that the distance between the vortex and antivortex in a V–AV pair is extremely small at zero temperature leading to large interactions between Majorana fermions locating at V–AV pairs. On the other hand, in traditional Zeeman induced FF superfluids, the transverse superfluid density is zero due to the rotational symmetry of the Fermi surface,[126,127] resulting in the zero critical temperature. However, Ref. 117 found nonzero and large critical temperatures for FF superfluids, gapless FF superfluids, topological FF superfluids and gapless topological FF superfluids in SO coupled Fermi gases. This paves the way for the experimental observation of 2D gapped and gapless FF superfluids and their associated topological excitations at finite temperature.

3.4. *Topological FF superfluids in 3D*

3.4.1. *Weyl fermions*

Weyl fermions[53] are massless chiral Dirac fermions with linear energy dispersions in momentum space, which can be described by Weyl equations:

$$H(\mathbf{k}) = \pm v\mathbf{k}\cdot\sigma\,, \tag{13}$$

where $\pm$ indicates the chirality of Weyl fermions. The masslessness can be understood from the fact that no fourth matrix can be found which anti-commutes with other three Pauli matrices. The spin expectation distribution of the occupied hole branch exhibits a hedgehog structure $\langle\sigma\rangle = \mp\mathbf{k}/k$ corresponding to the right-handed (left-handed) chirality.

Weyl fermions were first proposed for describing massless chiral Dirac fermions such as neutrinos in particle physics in 1929. Despite much effort, these fermions

have not yet been observed in experiments (neutrinos have mass). Recently, Weyl fermions have been suggested to exist in some solid state materials (i.e., Weyl semimetals), such as Pyrochlore Iridates,[128,129] ferromagnetic compound $HgCr_2Se_4$,[130] multilayer topological insulators,[131] photonic crystals,[132] as well as in optical lattices.[133,134] These materials possess the band touching points, around which the energy dispersions are linear. Such band touching points have to appear in pairs with opposite topological charge (i.e., chirality). Compared with 2D Dirac fermions (e.g., graphene), whose gap can be opened by perturbations that break time-reversal or spatial inversion symmetries, the gap of Weyl nodes cannot be opened unless two Weyl fermions with opposite topological charges are merged.

In solid materials, Weyl fermions exist in a single particle spectrum. It is natural to ask whether Weyl fermions can also exist in the quasiparticle excitation spectrum. The pioneer work in this issue is the proposal of Weyl fermions in ^{3}He A phase by Volovik.[54] However, ^{3}He is a strongly interacting system and very complicated to understand. Recently, Weyl fermions have been found in the quasiparticle excitation spectrum of SO coupled Fermi superfluids with simple s-wave interactions,[55,56] SO coupled FF superfluids,[57,58] nodal phases of $Cu_xBi_2Se_3$,[135] and dipolar Fermi gases.[59]

3.4.2. *BCS–BEC crossover and phase diagram*

Before we discuss the properties of Weyl fermions in a SO coupled Fermi gas, we first study the BCS–BEC crossover and then map out the zero temperature phase diagram. Figure 6 presents the order parameter Δ_0, chemical potential μ and Q_y with respect to $1/K_F a_s$. Δ_0 increases while μ decreases with increasing $1/K_F a_s$, leading to the same value independent of Zeeman fields (h_x, h_z) as the attractive interactions are sufficiently strong. This signals the crossover from BCS

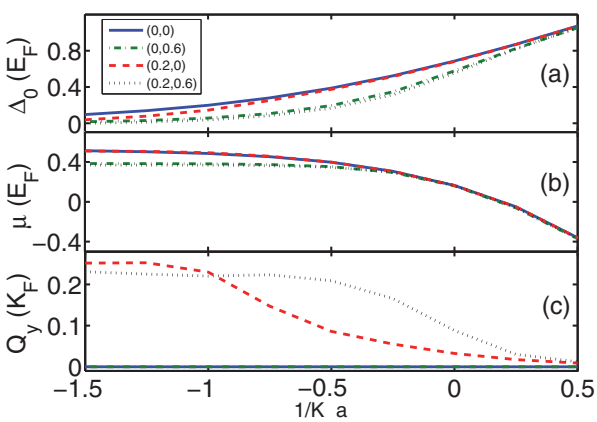

Fig. 6. (Color online) Plot of the order parameter Δ_0 in (a), chemical potential μ in (b) and Q_y in (c) as a function of $1/K_F a_s$ for different parameters (h_x, h_z). $\alpha K_F = E_F$ and the temperature $T = 0$. From Ref. 57.

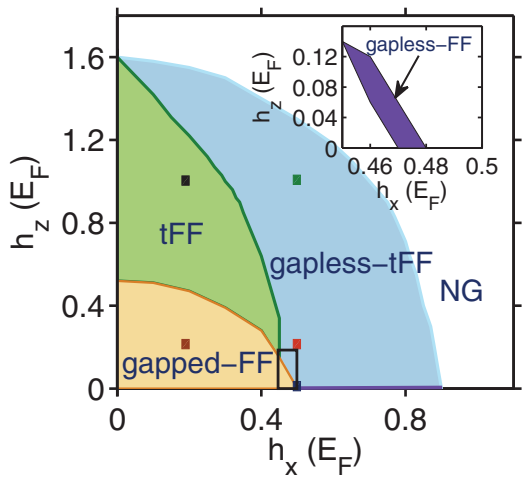

Fig. 7. (Color online) Zero temperature mean-field phase diagram of 3D SO coupled Fermi gases in the plane (h_x, h_z). The area in the small black box is enlarged in the inset, which shows the gapless FF phase. tFF: topological FF states; gapless-tFF: gapless topological FF state; NG: normal gas. Here $\alpha K_F = E_F$ and $1/a_s K_F = -0.1$.

superfluids to tightly bound molecule BEC superfluids. The finite momentum Q_y is nonzero when $h_x \neq 0$, indicating the superfluids are FF type. This Q_y is roughly a monotonously decreasing function of $1/K_F a_s$ in the sense that the momenta of Cooper pairs induced from weak interactions reflect the Fermi surface structure. Both Zeeman fields are detrimental to BCS paring, leading to the decreased Δ_0 when the total Zeeman field $h = \sqrt{h_x^2 + h_z^2}$ is larger. Since the physical quantities are independent of Zeeman fields on the BEC side, we focus on the FF superfluids on the BCS side.

In Fig. 7, the zero temperature phase diagram is mapped out in the plane (h_x, h_z). With pure h_x corresponding to the horizontal axis, the ground state is FF state when h_x is nonzero. Such FF states can be divided into two groups: gapped one with $E_g > 0$ and gapless one with $E_g < 0$, where the gap $E_g = \min(E_-^+)$ is defined as the minimum of the particle branch of the quasiparticle energy excitations. With increasing h_x, FF states transit from gapped one to gapless one. Such transition was first found in 2D in Ref. 90 and in 3D in Ref. 94. The gapless FF states are confirmed to be stable against phase fluctuations in both 2D[116,117] and 3D.[136,137] On the other hand, the superfluids can transit from normal superfluids to topological superfluids[55] in the presence of h_z but without h_x. With h_x, this transition is replaced by the transition from gapped FF states to topological FF states. In the topological FF phase, there exist band touching points (i.e., Weyl fermions) as well as FF Cooper pairs in the quasiparticle energy excitations. Interestingly, a large region of the phase diagram is occupied by a gapless topological FF superfluid with Weyl fermion excitations and $E_g < 0$. Instead, the gapless FF superfluids area becomes extremely small, which separates the gapped FF states

from the gapless topological FF superfluids. In 2D, the parameter region where such gapless FF superfluids including both gapless FF and gapless topological FF states exist becomes much smaller,[116,117] given that the gap at $k = 0$ begins increasing after its closing as h_z becomes larger.

3.4.3. *Linear quasiparticle excitation spectrum*

Weyl fermions possess linear energy dispersions. To check this, we first consider SO coupled Fermi gases subject to only out-of-plane Zeeman field h_z.[55] The quasiparticle energy excitations can be analytically written as

$$E_{\pm}^{\lambda}(\mathbf{k}) = \lambda\sqrt{\xi_{\mathbf{k}}^2 + \alpha^2 k_{\perp}^2 + h_z^2 + |\Delta_0|^2 \pm 2\sqrt{h_z^2(\xi_{\mathbf{k}}^2 + |\Delta_0|^2) + \alpha^2 k_{\perp}^2 \xi_{\mathbf{k}}^2}}\,, \tag{14}$$

where $\lambda = \pm$ indicating the particle $(+)$ and hole branches $(-)$ respectively, $\xi = \hbar^2\mathbf{k}^2/2m - \mu$ and $k_{\perp} = \sqrt{k_x^2 + k_y^2}$. Without SO coupling and Zeeman fields ($\alpha = h_z = 0$), it becomes the typical BCS superfluids excitations $E_{\mathbf{k},\pm}^{\lambda} = \lambda\sqrt{\xi_{\mathbf{k}}^2 + |\Delta_0|^2}$. In the previous subsection, we have discussed that in 2D the topological phase transition happens at the point across which the gap first closes and then reopens, generally signaling a sharp change of Chern number. In 3D, we cannot define Chern number in the whole momentum space. However, we can still find such gap close points. The kinetic energy $\hbar^2 k_z^2/2m$ along the z-direction can be incorporated into the chemical potential so that the excitation gap becomes $|\sqrt{(\mu - \hbar^2 k_z^2/2m)^2 + \Delta_0^2} - h_z|$. Clearly, when $h_z = |\Delta_0| = h_c$ $(\mu > 0)$, the gap closes. However, the gap keeps closed even with increasing h_z since k_z can vary. From $h_z = \sqrt{(\mu - \hbar^2 k_z^2/2m)^2 + \Delta_0^2}$, the gapless points exist at four points: $k_z = k_c = \pm\sqrt{\mu + \sqrt{h_z^2 - |\Delta_0|^2}}$ and $k_z = k_c = \pm\sqrt{\mu - \sqrt{h_z^2 - |\Delta_0|^2}}$, when $|\Delta_0| < h_z < \sqrt{\mu^2 + |\Delta_0|^2}$, and only two points: $k_z = k_c = \pm\sqrt{\mu + \sqrt{h_z^2 - |\Delta_0|^2}}$, when $h_z > \sqrt{\mu^2 + |\Delta_0|^2}$.

Around the zero energy point $\mathbf{k} = \mathbf{k}_W$ with $\mathbf{k}_W = (0, 0, k_c)$, the energy dispersion can be approximately written as

$$E_{-}^{\pm}(k_x = \delta k_x, k_y = 0, k_z = k_c) = \pm\frac{\alpha\Delta_0}{h_z}|\delta k_x|\,, \tag{15}$$

$$E_{-}^{\pm}(k_x = 0, k_y = 0, k_z = k_c + \delta k_z) = \pm\frac{\sqrt{2}\hbar^2|\xi_{\mathbf{k}_W} k_c|}{m\sqrt{\Delta_0^2 + \xi_{\mathbf{k}_W}^2}}\delta k_z\,. \tag{16}$$

Clearly, this spectrum is linear along all three directions. The anisotropy of the slope along the z-direction and the plane originates from the plane SO coupling of atoms. At the transition point where $k_c = 0$ or $\xi_{\mathbf{K}_W} = 0$, the liner behavior around the z-direction vanishes.

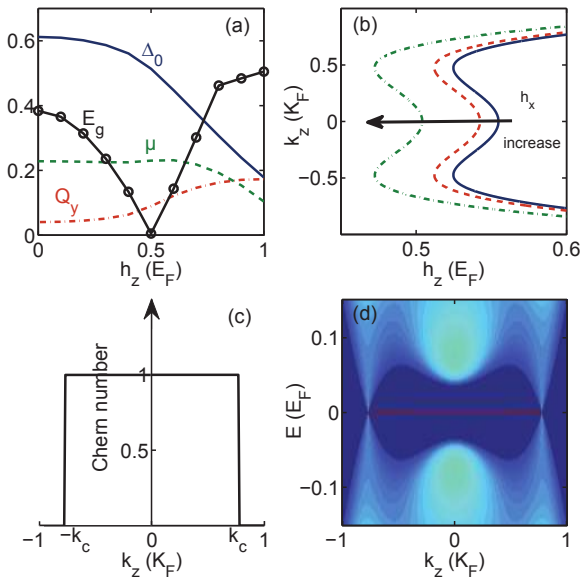

Fig. 8. (Color online) (a) Plot of order parameter Δ_0, Q_y, chemical potential μ and the quasiparticle excitation gap E_g at $k_z = 0$, as a function of h_z with $h_x = 0.2E_F$. (b) Gap closing points ($E_g = 0$) in the (h_z, k_z) plane for $h_x = 0$ (solid blue line), $h_x = 0.1E_F$ (dashed red line), and $h_x = 0.2E_F$ (dashed-dot green line). (c) Chern number for a fixed k_z plane. (d) The density of states at $k_y = 0$. The light blue region and the red line (Fermi arch) represent bulk and surface excitations, respectively. In (c) and (d), $h_x = 0.2E_F$, $h_z = 0.55E_F$. In all four figures $\alpha K_F = E_F$, $1/a_s K_F = -0.1$. From Ref. 57.

In the presence of in-plane Zeeman fields h_x, $Q_y \neq 0$ and the gap at $k_\perp = 0$ closes when

$$(h_x + \alpha Q_y/2)^2 + h_z^2 = (\hbar^2 k_z^2/2m - \bar{\mu})^2 + \Delta_0^2, \tag{17}$$

with $\bar{\mu} = \mu - Q_y^2/8m$. This equation determines the position $\mathbf{k}_W$ of the Weyl nodes. When $h_x = Q_y = 0$, it reduces to $h_z^2 = (\hbar^2 k_z^2/2m - \mu)^2 + \Delta_0^2$, exactly the same as previous results with only h_z. The gap at $k_z = 0$ first closes and then reopens as shown in Fig. 8(a). Across the gap closing point, the order parameter Δ_0 is still finite. The finite Q_y indicates the FF superfluids. Analogous to the system with pure h_z, there are two regions: $h_z > \sqrt{\bar{\mu}^2 + \Delta_0^2 - (h_x + \alpha Q_y/2)^2}$ with two zero excitations and $\sqrt{\Delta_0^2 - (h_x + \alpha Q_y/2)^2} < h_z < \sqrt{\bar{\mu}^2 + \Delta_0^2 - (h_x + \alpha Q_y/2)^2}$ and $\bar{\mu} > 0$ with four zero excitations. Both critical values for h_z decrease with increasing h_x as shown in Fig. 8(b). As h_x approaches such that $\Delta_0^2 = (h_x + \alpha Q_y/2)^2$, the topological transition occurs at $h_z = 0$ as shown in Fig. 7. Figure 8(b) also implies that the properties of Weyl fermions, such as the number, position and creating and annihilating, can be readily tuned through changing Zeeman fields.

Figure 9(a) presents the linear excitations cove along the k_x and k_y directions. The linear characteristic along the k_z direction can be seen from Fig. 8(d). It is important to note that the slope along different directions is different, indicating

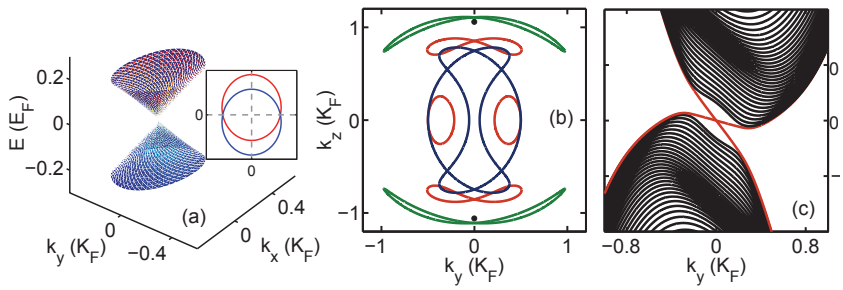

Fig. 9. (Color online) (a) Quasiparticle excitations around the Weyl node $\mathbf{k}_W = (0, 0, 0.77K_F)$ with $h_z = 0.55E_F$ and $h_x = 0.2E_F$. The contours of energy with $E = 0.1E_F$ (red line) and $E = -0.1E_F$ (blue line) are given in the inset. (b) Contours of zero energy quasiparticle spectrum in the plane (k_y, k_z) with $k_x = 0$. Here $h_x = 0.5E_F$, $h_z = 0$ (blue line), $h_z = 0.2E_F$ (red line), $h_z = E_F$ (green line) and $h_x = 0.2E_F$, $h_z = E_F$ (black points) correspond to blue, red, green, black square points, respectively in Fig. 7. There is no zero energy excitations for the brown point in the gapped FF phase. (c) Quasiparticle excitation spectrum in the gapless topological FF phase ($h_x = 0.5E_F$ and $h_z = 0.2E_F$) as a function of k_y with fixed $k_z = 0.8K_F$ and confinement in the x-direction. The black lines correspond to the bulk states while the red lines the surface states. Here $\alpha K_F = E_F$, $1/a_s K_F = -0.1$.

that these Weyl fermions are anisotropic. The difference along the z-direction originates from the anisotropic SO coupling, which only exists in the (x, y) plane. Such difference also exists even without h_x as seen from Eqs. (15) and (16). However, the difference between the slopes along x- and y-directions results from finite momentum FF pairings.

Alternatively, the systems with Weyl fermions can be regarded as stacks of quantum Hall insulators of quasiparticles in momentum space parameterized by k_z. Weyl fermions emerge at the edges between quantum Hall insulators and normal insulators, where Chern number changes sharply. In the topological FF phase, because the quasiparticle excitations are gapped (except at the Weyl nodes) in the 2D plane with a fixed k_z, we can calculate the Chern number for the hole branch for each k_z plane

$$C(k_z) = \frac{1}{2\pi} \sum_n \int dk_x dk_y \Omega^n(k_x, k_y) \,, \tag{18}$$

where n is the index for hole branches and the Berry curvature in the z-direction can be written as[138]

$$\Omega^n = i \sum_{n' \neq n} \left[\frac{\langle n|\partial_{k_x} H_B|n'\rangle\langle n'|\partial_{k_y} H_B|n\rangle - (k_x \leftrightarrow k_y)}{(E_{n\mathbf{k}} - E_{n'\mathbf{k}})^2} \right], \tag{19}$$

and n', which is not equal to n, runs over the eigenstates of H_B.

Figure 8(c) shows that when $|k_z| < k_c$, Chern number $C = 1$ and $C = 0$ otherwise. It is well-known that there exist chiral edge states between a quantum Hall insulator and a normal insulator. Thus, chiral edge states are expected to exist if the edges are imposed along the x- or y-direction for a fixed k_z, where Chern

number is nonzero. For instance, with the confinement along the x-direction, the edge states spectrum should intersect at $k_y = 0$ and $E = 0$. This results in a nonclosed Fermi surface (i.e., Fermi arch) connecting two Weyl points [shown in Fig. 8(d)], which consists of surface states. The Fermi arch can also be regarded as zero energy Majarona fermion flat band. We note that if the SO coupling is the equal Rashba–Dresshaul type, zero points form a loop in momentum space[85] and there exist a Majorana plane filling in the loop.[139]

3.4.4. *Gapless topological superfluids*

Topological FF superfluids are gapless and gapless excitations occur at a pair of points $\mathbf{k} = \mathbf{k}_W$ (i.e., Weyl points) where the particle and hole branches touch. However, with increasing h_x, the distortion of the quasiparticle excitations along the y-direction becomes sufficiently strong that the particle branch cuts the zero energy plane, leading to gapless FF superfluids ($E_g < 0$). Note that the minimum of the particle branch and the maximum of the hole branch do not generally occur at the same $\mathbf{k}$ because of the asymmetry induced by h_x corresponding to symmetry $\sigma_0 \otimes i\sigma_z\mathcal{K}$ broken with the complex conjugate operator $\mathcal{K}$. However, the particle-hole symmetry is still conserved, meaning that when the minimum of the particle branch occurs at $-\mathbf{k}$, the maximum of the hole branch occurs at $\mathbf{k}$. Such gapless FF superfluids can be topological or topological trivial, depending on whether there exist a pair of zero energy points where the particle and hole branches touch with the linear excitation dispersion and whether such pair of zero energy points is connected.

Figure 9(b) displays the zero energy contour of each gapless states. For topological FF states, there are two isolated points along the k_z-direction. For gapless topological FF states, such gapless points become closed loops connected at a Weyl point where the particle and hole branches touch. For gapless FF states (topological trivial), we can divide them into two groups depending on whether the state possesses the band touching points. Although the quasiparticle spectrum of one group has the touching points with linear dispersions [see the blue line in Fig. 9(b)], it does not exhibit any topological properties. To confirm that the touching points in gapless topological FF superfluids are indeed Weyl fermions, we calculate the Chern number of the hole branches and find that it is nonzero when k_z lies between those two points and zero otherwise. Figure 9(c) illustrates the surface states (red line) with the confinement along the x direction. Such surface states can still form the zero energy Fermi arch similar to Fig. 8(d).

For an isotropic SO coupled Fermi gas subject to Zeeman fields, there only exist gapless topological superfluids,[58] but not topological superfluids, in the sense that the same Zeeman field not only generates Weyl points but also creates FF pairings, in contrast to Rashba SO coupled Fermi gas where the Zeeman field perpendicular to the SO coupling plane generates Weyl points and the Zeeman field in the plane creates FF pirings. The surface states are visualized in real space in Ref. 58.

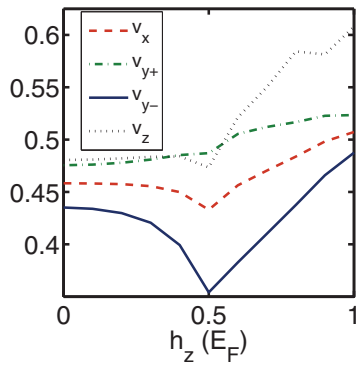

Fig. 10. (Color online) Sound speeds as a function of h_z. Dashed red and dotted black lines represent the speed along x- and z-directions. Solid blue and dashed-dot green lines represent sound speeds along negative y and positive y-directions, respectively. The unit of sound speed is $v_F = \hbar K_F/m$. Here $h_x = 0.2E_F$, $\alpha K_F = E_F$, and $1/a_s K_F = -0.1$. From Ref. 57.

3.5. *Sound speeds as an experimental signal*

FF superfluids have finite center-of-mass momentum Cooper pairs. To detect such exotic states in experiments, the direct method is to probe the momenta of Cooper pairs. In cold atom systems, such finite momenta can be reflected by the pair momentum distribution after the time-of-flight expansion.[18,19] Other indirect methods, such as noise correlations,[140] have also been suggested. However, to date, in cold atom experiments, only the density profiles of both components have been measured. This experiment only partially confirms the existence of FFLO superfluids.

Sound modes which have linear energy dispersions are the collective excitations excited by density fluctuations. The speeds of sound are defined as the slopes of the linear dispersion, which reflect the robustness of superfluidity in superfluids/superconductors. For instance, in BECs, the critical velocity to destroy superfluidity is determined by sound speeds. In the BCS superfluids, although the speeds of sound are generally larger than the velocity defined by the gap, they can still be experimentally measured[141,142] by observing the propagation of a localized density perturbation created by a laser beam. In this subsection, we suggest that the speeds of sound can be employed as a signal[143,144] reflecting the topological phase transition from gapped FF superfluids to topological FF superfluids.[57]

In Fig. 10, we plot the speeds of sound along each direction with respect to h_z corresponding to the transition from gapped FF superfluids to topological FF superfluids. The speeds of sound are anisotropic in all different directions. The anisotropy between the z-direction and the (x, y) plane comes from the SO coupling and the anisotropy in the plane comes from the finite momentum pairings. They are anisotropic even in the positive and negative y-directions, reflecting the existence of FF superfluids. In addition, there is a minimum in the speeds of sound at the topological transition point where quantum fluctuations are relatively strong. This signal may be used to measure the topological transition in experiments.

4. Conclusion

In this review, we discussed the topological properties of FF superfluids in both low dimensions and 3D. The mechanism of FF superfluids is completely different from the traditional Zeeman field induced FFLO superfluids. Here the FF superfluids originate from the symmetry breaking of the single particle band structure induced by SO coupling and in-plane Zeeman fields. In low dimensions, such FF superfluids can become topological when an out-of-Zeeman field is included. In the topological FF superfluids, Majorana fermions are locally accommodated in real space. The finite BKT temperature paves the way for experimentally observing the Majorana fermions as well as FF type pairings in 2D. In 3D, an out-of-Zeeman field can still drive the system into a topological state. Compared with 2D, the topology is essentially reflected by the emergence of Weyl fermions in momentum space. Such Weyl fermions can be different from traditional ones in the sense that the quasiparticle excitations become gapless except the Weyl points. In experiments, the speeds of sound may provide an effective approach to probe the topological FF states.

Acknowledgments

We thank Z. Zheng, C. Qu and K. Sun for helpful discussion and critical reading. Y. Xu and C. Zhang are supported by ARO(W911NF-12-1-0334), AFOSR (FA9550-13-1-0045) and NSF-PHY (1249293).

References

1. P. Fulde and R. A. Ferrell, *Phys. Rev.* **135**, A550 (1964).
2. A. I. Larkin and Yu. N. Ovchinnikov, *Zh. Eksp. Teor. Fiz.* **47**, 1136 (1964) [*Sov. Phys. JETP* **20**, 762 (1965)].
3. H. A. Radovan *et al.*, *Nature* **425**, 51 (2003).
4. A. Bianchi *et al.*, *Phys. Rev. Lett.* **91**, 187004 (2003).
5. K. Kakuyanagi *et al.*, *Phys. Rev. Lett.* **94**, 047602 (2005).
6. Y. Matsuda and H. Shimahara, *J. Phys. Soc. Jpn.* **76**, 051005 (2007).
7. M. Kenzelmann *et al.*, *Science* **321**, 1652 (2008).
8. S. Uji *et al.*, *Phys. Rev. Lett.* **97**, 157001 (2006).
9. R. Lortz *et al.*, *Phys. Rev. Lett.* **99**, 187002 (2007).
10. B. Bergk *et al.*, *Phys. Rev. B* **83**, 064506 (2011).
11. W. A. Coniglio *et al.*, *Phys. Rev. B* **83**, 224507 (2011).
12. K. Cho *et al.*, *Phys. Rev. B* **83**, 060502(R) (2011).
13. A. Ptok and D. Crivelli, *J. Low Temp. Phys.* **172**, 226 (2013).
14. L. Li *et al.*, *Nature* **7**, 762 (2011).
15. D. E. Sheehy and L. Radzihovsky, *Phys. Rev. Lett.* **96**, 060401 (2006).
16. M. M. Parish *et al.*, *Nat. Phys.* **3**, 124 (2007).
17. J. P. A. Devreese and J. Tempere, arXiv:1310.3840v1.
18. T. K. Koponen *et al.*, *Phys. Rev. Lett.* **99**, 120403 (2007).
19. A. E. Feiguin and F. Heidrich-Meisner, *Phys. Rev. B* **76**, 220508(R) (2007).
20. Q. Cui and K. Yang, *Phys. Rev. B* **78**, 054501 (2008).
21. Y. Chen *et al.*, *Phys. Rev. B* **79**, 054512 (2009).

22. Y. L. Loh and N. Trivedi, *Phys. Rev. Lett.* **104**, 165302 (2010).
23. Z. Cai, Y. Wang and C. Wu, *Phys. Rev. A* **83**, 063621 (2011).
24. M. J. Wolak *et al.*, *Phys. Rev. A* **86**, 023630 (2012).
25. G. Orso, *Phys. Rev. Lett.* **98**, 070402 (2007).
26. H. Hu, X.-J. Liu and P. D. Drummond, *Phys. Rev. Lett.* **98**, 070403 (2007).
27. M. M. Parish *et al.*, *Phys. Rev. Lett.* **99**, 250403 (2007).
28. E. Zhao and W. V. Liu, *Phys. Rev. A* **78**, 063605 (2008).
29. M. Casula, D. M. Ceperley and E. J. Mueller, *Phys. Rev. A* **78**, 033607 (2008).
30. Z.-J. Ying *et al.*, *Phys. Rev. Lett.* **100**, 140406 (2008).
31. M. Tezuka and M. Ueda, *Phys. Rev. Lett.* **100**, 110403 (2008).
32. K. Sun *et al.*, *Phys. Rev. A* **83**, 033608 (2011).
33. K. Sun and C. J. Bolech, *Phys. Rev. A* **85**, 051607(R) (2012).
34. A. E. Feiguin *et al.*, *Lect. Notes Phys.* **836**, 503 (2012).
35. X.-W. Guan, M. T. Batchelor and C. Lee, *Rev. Mod. Phys.* **85**, 1633 (2013).
36. K. Yang, *Phys. Rev. B* **63**, 140511(R) (2001).
37. Y.-A. Liao *et al.*, *Nature* **467**, 567 (2010).
38. N. Read and D. Green, *Phys. Rev. B* **61**, 10267 (2000).
39. T. Mizushima, M. Ichioka and K. Machida, *Phys. Rev. Lett.* **101**, 150409 (2008).
40. L. Fu and C. L. Kane, *Phys. Rev. Lett.* **100**, 096407 (2008).
41. C. Nayak *et al.*, *Rev. Mod. Phys.* **80**, 1083 (2008).
42. J. D. Sau *et al.*, *Phys. Rev. Lett.* **104**, 040502 (2010).
43. R. M. Lutchyn, J. D. Sau and S. DasSarma, *Phys. Rev. Lett.* **105**, 077001 (2010).
44. Y. Oreg, G. Refael and F. von Oppen, *Phys. Rev. Lett.* **105**, 177002 (2010).
45. X. L. Qi and S. C. Zhang, *Rev. Mod. Phys.* **83**, 1057 (2011).
46. J. Alicea, *Rep. Prog. Phys.* **75**, 076501 (2012).
47. V. Mourik *et al.*, *Science* **336**, 1003 (2012).
48. M. T. Deng *et al.*, *Nano Lett.* **12**, 6414 (2012).
49. A. Das *et al.*, *Nat. Phys.* **8**, 887 (2012).
50. L. P. Rokhinson, X. Liu and J. K. Furdyna, *Nat. Phys.* **8**, 795 (2012).
51. Y. Li, D. Wang and C. Wu, *New J. Phys.* **15**, 085002 (2013).
52. A. Kitaev, *Ann. Phys.* (*N.Y.*) **303**, 2 (2003).
53. H. Weyl, *Zeitschrift für Physik* **56**, 330 (1929).
54. G. E. Volovik, in *The Universe in a Helium Droplet* (Clarendon Press, Oxford, 2003).
55. M. Gong, S. Tewari and C. Zhang, *Phys. Rev. Lett.* **107**, 195303 (2011).
56. K. Seo, C. Zhang and S. Tewari, *Phys. Rev. A* **87**, 063618 (2013).
57. Y. Xu, R.-L. Chu and C. Zhang, *Phys. Rev. Lett.* **112**, 136402 (2014).
58. H. Hu *et al.*, arXiv:1404.2442.
59. B. Liu *et al.*, arXiv:1407.2949.
60. Y.-J. Lin, K. Jiménez-García and I. B. Spielman, *Nature* (*London*) **471**, 83 (2011).
61. P. Wang *et al.*, *Phys. Rev. Lett.* **109**, 095301 (2012).
62. L. W. Cheuk *et al.*, *Phys. Rev. Lett.* **109**, 095302 (2012).
63. J.-Y. Zhang *et al.*, *Phys. Rev. Lett.* **109**, 115301 (2012).
64. C. Qu *et al.*, *Phys. Rev. A* **88**, 021604(R) (2013).
65. R. A. Williams *et al.*, *Phys. Rev. Lett.* **111**, 095301 (2013).
66. W. Yi, W. Zhang and X. Cui, arXiv:1410.1595.
67. J. Dalibard *et al.*, *Rev. Mod. Phys.* **83**, 1523 (2011).
68. H. Zhai, *Int. J. Mod. Phys. B* **26**, 1230001 (2012).
69. V. Galitski and I. B. Spielman, *Nature* (*London*) **494**, 49 (2013).
70. X. Zhou *et al.*, *J. Phys. B: At. Mol. Opt. Phys.* **46**, 134001 (2013).
71. C. Wang *et al.*, *Phys. Rev. Lett.* **105**, 160403 (2010).

72. T. D. Stanescu, B. Anderson and V. Galitski, *Phys. Rev. A* **78**, 023616, (2008).
73. C. Wu, I. Mondragon-Shem and X. F. Zhou, *Chin. Phys. Lett.* **28**, 097102 (2011).
74. Y. Zhang, L. Mao and C. Zhang, *Phys. Rev. Lett.* **108**, 035302 (2012).
75. S. Sinha, R. Nath and L. Santos, *Phys. Rev. Lett.* **107**, 270401 (2011).
76. H. Hu *et al.*, *Phys. Rev. Lett.* **108**, 010402 (2012).
77. Y. Xu, Y. Zhang and B. Wu, *Phys. Rev. A* **87**, 013614 (2013).
78. V. Achilleos *et al.*, *Phys. Rev. Lett.* **110**, 264101 (2013).
79. Q. Zhu, C. Zhang and B. Wu, *Europhys. Lett.* **100**, 50003 (2013).
80. C. Zhang *et al.*, *Phys. Rev. Lett.* **101**, 160401 (2008).
81. M. Sato, Y. Takahashi and S. Fujimoto, *Phys. Rev. Lett.* **103**, 020401 (2009).
82. S.-L. Zhu *et al.*, *Phys. Rev. Lett.* **106**, 100404 (2011).
83. L. Jiang *et al.*, *Phys. Rev. Lett.* **106**, 220402 (2011).
84. X.-J. Liu and H. Hu, *Phys. Rev. A* **85**, 033622 (2012).
85. K. Seo, L. Han and C. A. R. Sá de Melo, *Phys. Rev. Lett.* **109**, 105303 (2012).
86. M. Gong *et al.*, *Phys. Rev. Lett.* **109**, 105302 (2012).
87. X.-J. Liu, K. T. Law and T. K. Ng, arXiv:1304.0291.
88. Y. Xu *et al.*, *Phys. Rev. Lett.* **113**, 130404 (2014).
89. Z. Zheng *et al.*, *Phys. Rev. A* **87**, 031602(R) (2013).
90. F. Wu *et al.*, *Phys. Rev. Lett.* **110**, 110401 (2013).
91. Z. Zheng *et al.*, arXiv:1212.6826.
92. X.-J. Liu and H. Hu, *Phys. Rev. A* **87**, 051608(R) (2013).
93. Z. Fu *et al.*, *Phys. Rev. A* **87**, 053619 (2013).
94. L. Dong, L. Jiang and H. Pu, *New J. Phys.* **15**, 075014 (2013).
95. H. Hui and X.-J. Liu, *New J. Phys.* **15**, 093037 (2013).
96. M. Iskin, *Phys. Rev. A* **88**, 013631 (2013).
97. L. Jiang *et al.*, arXiv:1404.6211.
98. Y. Xu *et al.*, *Phys. Rev. A* **89**, 013607 (2014).
99. C. Qu *et al.*, *Nat. Commun.* **4**, 2710 (2013).
100. W. Zhang and W. Yi, *Nat. Commun.* **4**, 2711 (2013).
101. X.-J. Liu and H. Hu, *Phys. Rev. A* **88**, 023622 (2013).
102. C. Chen, *Phys. Rev. Lett.* **111**, 235302 (2013).
103. S. Giorgini, L. P. Pitaevskii and S. Stringari, *Rev. Mod. Phys.* **80**, 1215 (2008).
104. A. Y. Kitaev, *Phys. Usp* **44**, 131 (2001).
105. L. M. Wong and K. T. Law, *Phys. Rev. B* **86**, 184516 (2012).
106. F. Zhang, C. L. Kane and E. J. Mele, *Phys. Rev. Lett.* **111**, 056402 (2013).
107. S. Nakosai *et al.*, *Phys. Rev. Lett.* **110**, 117002 (2013).
108. A. Keselman *et al.*, *Phys. Rev. Lett.* **111**, 116402 (2013).
109. X.-J. Liu, C. L. M. Wong and K. T. Law, *Phys. Rev. X* **4**, 021018 (2014).
110. C. Qu, M. Gong and C. Zhang, *Phys. Rev. A* **89**, 053618 (2014).
111. B. Liu *et al.*, arXiv:1402.5995.
112. Z. Zheng *et al.*, arXiv:1408.5824.
113. J. Liu *et al.*, *Phys. Rev. Lett.* **109**, 267002 (2012).
114. P. Ghosh *et al.*, *Phys. Rev. B* **82**, 184525 (2010).
115. C. Chan and M. Gong, *Phys. Rev. B* **89**, 174501 (2014).
116. Y. Cao *et al.*, arXiv:1402.6832.
117. Y. Xu and C. Zhang, arXiv:1407.3483.
118. L. Fidkowski *et al.*, *Phys. Rev. B* **84**, 195436 (2011).
119. J. D. Sau *et al.*, *Phys. Rev. B* **84**, 144509 (2011).
120. V. L. Berezinskii, *Sov. Phys. JETP* **32**, 493 (1971).
121. J. M. Kosterlitz and D. Thouless, *J. Phys. C* **5**, L124 (1972).

122. J. M. Kosterlitz and D. Thouless, *J. Phys. C* **6**, 1181 (1973).
123. S. S. Botelho and C. A. R. Sá de Melo, *Phys. Rev. Lett.* **96**, 040404 (2006).
124. L. He and X.-G. Huang, *Phys. Rev. Lett.* **108**, 145302 (2012).
125. J. P. A. Devreese, J. Tempere and C. A. R. Sà de Melo, *Phys. Rev. Lett.* **113**, 165304 (2014).
126. L. Radzihovsky and A. Vishwanath, *Phys. Rev. Lett.* **103**, 010404 (2009).
127. S. Yin, J.-P. Martikainen and P. Törmä, *Phys. Rev. B* **89**, 014507 (2014).
128. X. Wan *et al.*, *Phys. Rev. B* **83**, 205101 (2011).
129. V. Aji, *Phys. Rev. B* **85**, 241101(R) (2012).
130. G. Xu *et al.*, *Phys. Rev. Lett.* **107**, 186806 (2011).
131. A. A. Burkov and L. Balents, *Phys. Rev. Lett.* **107**, 127205 (2011).
132. L. Lu *et al.*, *Nat. Photon.* **7**, 294 (2013).
133. D. Bercioux *et al.*, *Phys. Rev. A* **80**, 063603 (2009).
134. Z. Lan, N. Goldman and P. Öhberg, *Phys. Rev. B* **85**, 155451 (2012).
135. S. A. Yang, H. Pan and F. Zhang, *Phys. Rev. Lett.* **113**, 046401 (2014).
136. X.-J. Liu, *Phys. Rev. A* **88**, 043607 (2013).
137. Z. Zheng *et al.*, arXiv:1407.3203 (2014).
138. D. Xiao, M.-C. Chang and Q. Niu, *Rev. Mod. Phys.* **82**, 1959 (2010).
139. C. Qu *et al.*, arXiv:1310.7557.
140. T. Paananen *et al.*, *Phys. Rev. A* **77**, 053602 (2008).
141. M. R. Andrews *et al.*, *Phys. Rev. Lett.* **79**, 553 (1997).
142. J. Joseph *et al.*, *Phys. Rev. Lett.* **98**, 170401 (2007).
143. M. O. J. Heikkinen and P. Törmä, *Phys. Rev. A* **83**, 053630 (2011).
144. L. He and X. G. Huang, *Phys. Rev. A* **86**, 043618 (2012).